In: IEEE International Conference on Robotics and Automation (ICRA 2006)
Orlando, Florida, USA, May 15th-19th 2006

Discontinuity Detection for Force-based Manipulation

Antoine SCHLECHTER and Dominik HENRICH

Lehrstuhl Angewandte Informatik III
Fakultät für Mathematik, Physik und Informatik
Universität Bayreuth, D-95445 Bayreuth, Germany
[Antoine.Schlechter | Dominik.Henrich] @ uni-bayreuth.de, Http: //ai3.inf.uni-bayreuth.de/

Abstract – In manipulation, workpieces have to be placed in an exact relationship to other objects that usually constrain the possible motions of the workpiece. Thus, control of a manipulation task can often be done by detecting the changes in the set of constraints acting on the workpiece. In the case of hard positional constraints on rigid objects, the detection can be done using simple thresholds on measured forces and/or moments. When some of these constraints are non-rigid (i. e. elastic) (Fig. 1), forces and moments vary during motions even if there is no change in the constraints, making it difficult if not impossible to find appropriate thresholds for forces and moments. In such situations changes in the constraints mostly lead to discontinuities (i. e. jumps and corners) in the measured force and moment signals. This paper presents a constant time algorithm for jump and corner detection in 1-dimensional sensor signals.

Index Terms – discontinuity detection, corner detection, jump detection, force-based manipulation, stationary robots

I. INTRODUCTION

When manipulating objects, the main issue is to change the set of constraints acting on the manipulated objects, i.e. to change the number of degrees of freedom for the objects motions. According to [5], the performance of assembly tasks can be regarded as stepwise increasing the number of constraints for one of the mating parts by establishing contact with other parts. A lot of research introduces contact states to describe differently constrained situations [1-3], [6], [11]. Even if some of these work address the difficult tasks to clearly distinct between different situations or contact states, it is often sufficient to detect the transition when the current contact situation changes in some way.

For handling rigid objects in a rigid environment, changes in the number of degrees of freedom can be detected by simple thresholds on the forces and moments measured during the manipulation operations. This approach to monitoring manipulation tasks is included in commercial robot controllers with a force option already (e.g. “guarded mode” in Adept V+ controllers or end conditions like “FCCond-Force” in ABB RAPID controllers).

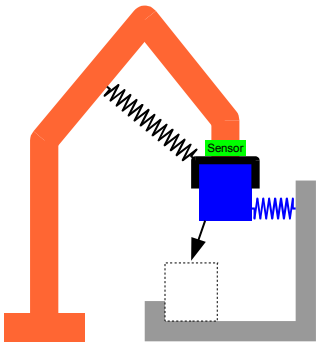

Fig. 1: Elastic constraints may disturb the forces used to control a manipulation task

If the manipulated object or the environment are non-rigid, there may be elastic constraints acting on the workpiece (Fig. 1). Elastic constraints can be found when manipulating elastically deformable objects, when a rigid workpiece is already fixed to some elastically deformable object, or when elastically deformable cables, ropes, hoses or wires are attached to the robot tool (or gripper) for its supply and control.

As the robot moves, elastic constraints produce changing forces and moments even if the set of constraints remains unchanged making it difficult to choose universally safe and reliable thresholds for forces and moments directly.

An example for a manipulation under elastic constraints is illustrated in Fig. 2. A polyamid hose that is threaded through a hole (left side in the picture) has to be threaded through a slot in a plate (right side in the background of the picture). In order to achieve this, the endpoint of the hose is first localized on the plate by drawing it over the right side edge onto the

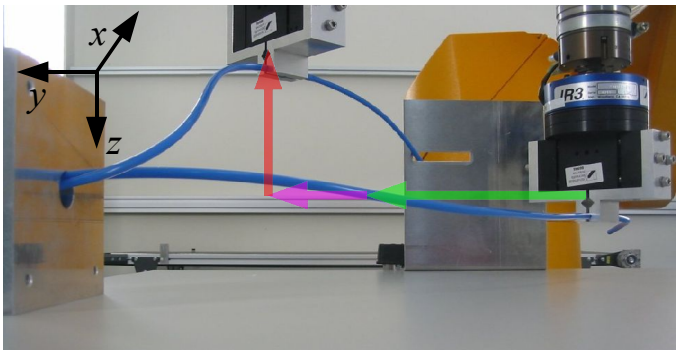

Fig. 2: The endpoint of a hose (blue) is first localised on the rear plate by drawing it over the right edge of the plate (green arrow). A transfer motion (magenta arrow) moves the endpoint beneath the slot in the rear plate.The endpoint is drawn over the downside edge into the slot (red arrow).

plate. A new constraint to the hose's motion is added when the right edge of the plate is contacted. As the robot moves parallel to the plate, the effect of this additional constraint on the hose's motion slowly diminishes and finally disappears, when the endpoint moves over the edge. Assuming these two changes in the set of constraints can be detected, the endpoint is localized near the edge of the plate, allowing to move the endpoint underneath the slot by a simple transfer motion with a fixed distance. From here, the endpoint is moved upwards until the remaining constraint of the endpoint sliding over the face spontaneously disappears when the endpoint drops into the slot.

The low-pass filtered forces and moments for three different runs of this experiment are depicted in Fig. 3. The contacting of the right side edge of the plate can be seen by the corners in the *Fy* force and in the *Mz* moment at 60 mm from the robots starting position. The endpoint sliding onto the face can be seen by the jumps in the *Fy* force and the corners in the *Mz* moment at 170 mm or 185 mm, depending on the run. The insertion of the endpoint into the slot can be seen by the jumps in the *Fx* force and *Mz* moment at 60 mm, 110 mm or 120mm, depending on the run. The large irregularities in these later signals are caused by friction in the first hole and on the plate.

In general, due to slightly different initial bendings, material parameters, or gripping positions, the location of the changes in constraints as well as the forces or moments produced by elastic constraints vary from situation to situation, making it difficult to select the right universal thresholds without risking damage or false alarms. In some situations, the changes in a set of constraints cannot be monitored by a threshold for forces and moments at all, because they reach their extrema exactly at or even before the change of the constraining situation (see Fig. 3 for examples).

In general, all elastic constraints produce variable forces and moments while the robot moves. If some, not necessarily

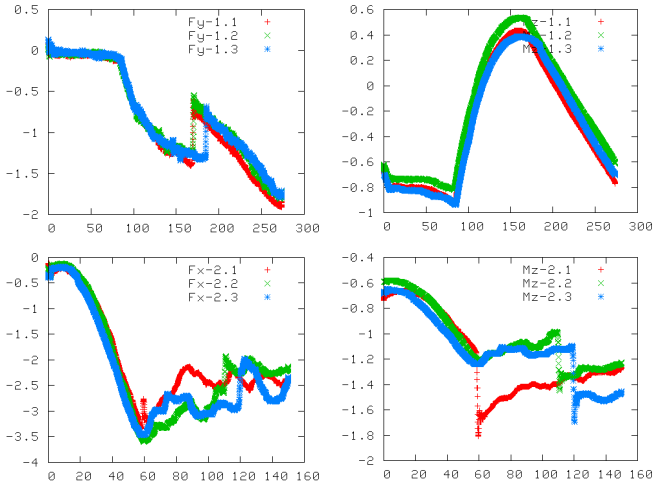

Fig. 3: Relevant forces and moments for three different runs of the experiment from Fig. 2. The forces *Fy* (upper left) and moments *Mz* (upper right) for the endpoint location on the plate, the forces *Fx* (lower left) and moments *Mz* (lower right) for the insertion of the endpoint into the slot. High resolution pictures may be downloaded from http://ai3.inf.uni-bayreuth.de/projects/rodeo/

elastic, constraint is added (or removed) at some position during the robot motion, the effect of this additional (or lost) constraint will be a discontinuity in some derivative of the signal. If a constraints vanishes spontaneously, we observe signal discontinuities, so called *jumps*, directly in the force or moment signal. In all other situations, discontinuities in the first derivative of the signal, so called *corners*, are most probable to be observed.

Thus, jumps and corners indicate changes in the current constraint situation and, consequently, the detection of such discontinuities enables the control of manipulation tasks as described in [7] or [9] for instance. In fact, discontinuity detection can be applied to all situations, where the relevant changes do be detected can be described using the L-function formalism described in [1].

The rest of the paper is organized as follows: Section II summarizes the state of the art concerning the detection of discontinuities, Section III describes our algorithm to find jumps and corners in one-dimensional signals and Section IV presents the performance of our algorithm on filtered and unfiltered data taken from the presented example manipulation.

II. State of the art

The problem of discontinuity detection has already been addressed before. In [9], an algorithm based on the extrapolation of the prediction band of a linear regression onto the signal is described. It performs acceptably for signals that are linear before the discontinuity. Curved signals often lead to false alarms, as the signal curvature may be seen as corners.

The equiarcide points algorithm described in [7] uses data of different statistic quality leading to a scale dependency of the algorithm. Additionally, good performance of the algorithm relies on a maximum to maximum and minimum to minimum filter [8], leading to an evaluation of the input signal in blocks of mostly unpredictable length, and thus to signal dependent delays in the detection of discontinuities.

In [4], pairs of a filter and a pattern are constructed for different types of discontinuities. The presence of the scaled pattern in the response of the signal to the corresponding filter indicates a discontinuity of the specified type. Both, the filter response and the check for the presence of the pattern are calculated by convolution, leading to a computational complexity in the order of the length of the filter and of the pattern for each new measurement.

III. Discontinuity Detection

Let us assume that the signal of interest is sampled at discrete points in time t and that the samples (x_t, y_t) follow a piecewise linear function corrupted by white noise n with mean $E(n) = 0$ and variance $V(n) = \sigma_n^2$:

$$y_t = \begin{cases} a_l x_t + b_l + n & x_t \le x^* \\ a_r x_t + b_r + n & x^* < x_t \end{cases} \qquad (1)$$

This assumption holds for all real signals at least in some small neighborhood around the discontinuity x^*.

In the case of force-based manipulation, the moments and forces are influenced by the robot position or configuration relative to the constraints, thus, the force measurements y_t are a function of some distance x_t of the current robot position to the starting position.

Given an arbitrary signal y_t according to (1) and an interval of $N+M$ consecutive samples (x_t, y_t) prior to some point in time t_0, detection of a discontinuity can be done by estimating a_l, a_r, b_l and b_r and rejecting the hypothesis H_0: $a_l = a_r \wedge b_l = b_r$. This can be done by finding evidence for one of the alternatives "positive corner" (H_{C+}: $a_l < a_r$), "negative corner" (H_{C-}: $a_l > a_r$), "positive jump" (H_{J+}: $b_l < b_r$) or "negative jump" (H_{J-}: $b_l > b_r$).

A. Jump Detection

In order to reject H_0 by confirming one of the jump alternatives, an ideal jump J_t (Fig. 4, left) of size Δ_b with discontinuity at $t_0 - M$ is fitted to the measured signal at each point in time t_0.

$$J_t = \begin{cases} a\,x_t + b & t_0 - N - M + 1 \le t \le t_0 - M \\ a\,x_t + b + \Delta_b & t_0 - M + 1 \le t \le t_0 \end{cases}$$

In the subsequent calculations, we will use the notations

$$\begin{aligned} &L_x = \sum_{t=t_0-N-M+1}^{t_0-M} x_t,\quad L_y = \sum_{t=t_0-N-M+1}^{t_0-M} y_t\quad L_{xx} = \sum_{t=t_0-N-M+1}^{t_0-M} x_t^2, \\ &L_{xy} = \sum_{t=t_0-N-M+1}^{t_0-M} x_t y_t, R_x = \sum_{t=t_0-M+1}^{t_0} x_t,\quad R_y = \sum_{t=t_0-M+1}^{t_0} y_t \\ &R_{xx} = \sum_{t=t_0-M+1}^{t_0} x_t^2,\quad R_{xy} = \sum_{t=t_0-M+1}^{t_0} x_t y_t \quad \text{and} \quad S_* = L_* + R_* \end{aligned} \tag{2}$$

Note that those sums can all be updated in constant time by adding each new sample to the different sums and to a buffer and subsequently removing the oldest sample from the sums and from the buffer.

The parameters a, b, and Δ_b are calculated by minimizing the sum of squared errors (SSE):

$$\mathrm{SSE}_J = \sum_{t=t_0-N-M+1}^{t_0} (y_t - J_t)^2 \tag{3}$$

Using the notations from (2), we find:

$$a = \frac{NM\,S_{xy} - M\,L_x L_y - N\,R_x R_y}{d_J}$$

$$b = \frac{L_x\left(R_x R_y - M\,S_{xy}\right) - L_y\left(R_x^2 - M\,S_{xx}\right)}{d_J}$$

$$\Delta_b = \left|\begin{array}{l}(R_x L_y - L_x R_y) S_x + (N\,R_y - M\,L_y) S_{xx} \\ \quad + (M\,L_x - N\,R_x) S_{xy}\end{array}\right| / d_J$$

$$d_J = NM\,S_{xx} - M\,L_x^2 - N\,R_x^2 \tag{4}$$

Under the hypothesis H_0, Δ_b is an unbiased estimator for the jump size $E(\Delta_b) = 0 = b_r - b_l$ with variance

$$V(\Delta_b) = \frac{(N+M)\,S_{xx} - S_x^2}{N\,M\,S_{xx} - N\,R_x^2 - M\,L_x^2}\,\sigma_n^2 \tag{5}$$

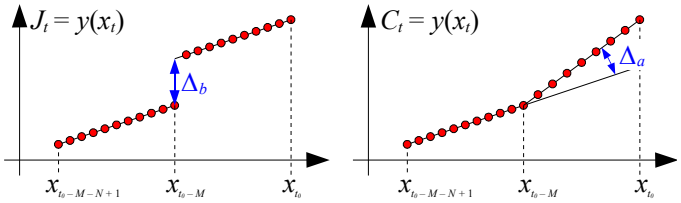

Fig. 4: Ideal jump J_t (left) and ideal corner C_t (right) to be fitted to the past $N+M$ measurement samples $y(x_t)$ at each point in time t_0.

If the signal noise is normally distributed, the estimate $\mathrm{SSE}_J / (N+M-3)$ for σ_n^2 has a χ^2–distribution with $N+M-3$ degrees of freedom. Thus, using this estimate for σ_n^2 the following test statistic t_J has a Student's t-distribution with $N+M-3$ degrees of freedom

$$t_J := \frac{\Delta_b}{\sqrt{V(\Delta_b)}} \tag{6}$$

In order to confirm a jump at some point in time $t_0 - M$, we need evidence for either the alternative that there is a positive jump H_{J+}: $\Delta_b > 0$ or the alternative that there is a negative jump H_{J-}: $\Delta_b < 0$ or the two-tailed alternative that there is some kind of a jump H_J: $\Delta_b \neq 0$. This hypothesis test can be done at a desired confidence level α by choosing a threshold for t_J in a way that the type-I error probability of deciding in favor of some kind of discontinuity (H_{J+}, H_{J-}, or H_J) if there is none will be α. With t_β being the percentage point of the student's t-distribution for a given probability β, the thresholds for the test statistic t_J can be summarized in the following rejection regions for the H_0 hypothesis:

$$\begin{aligned} H_0 &: a_l = a_r \wedge \Delta_b = 0 \\ H_{J+} &: \Delta_b > 0 \quad \text{accept if} \quad t_J > t_{1-\alpha} \\ H_{J-} &: \Delta_b < 0 \quad \text{accept if} \quad t_J < -t_{1-\alpha} \\ H_J &: \Delta_b \neq 0 \quad \text{accept if} \quad |t_J| > t_{1-\alpha/2} \end{aligned} \tag{7}$$

If the measurement noise is not normally distributed, for instance when using low pass filtered force-data, we have to choose an application specific threshold for t_J or for Δ_b directly based on the real noise distribution.

B. Corner Detection

In order to reject H_0 by confirming one of the corner alternatives, an ideal corner C_t (Fig. 4, right) of size Δ_a with discontinuity at $t_0 - M$ is fitted to the measured signal at each point in time t_0.

$$C_t = \begin{cases} a\,x_t + b & t_0 - N - M + 1 \le t \le t_0 - M \\ (a + \Delta_a)\,x_t - \Delta_a\,x_{t_0-M} + b & t_0 - M + 1 \le t \le t_0 \end{cases}$$

The parameters a, b, and Δ_a are calculated by minimizing the sum of squared errors

$$\mathrm{SSE}_C = \sum_{t=t_0-N-M+1}^{t_0} (y_t - C_t)^2 \tag{8}$$

Using the notations from (2), we find:

$$\begin{aligned}\Delta_a = &\big|\big((M L_y - N R_y) S_{xx} + (N R_x - M L_x) S_{xy} \\ &+ (L_x R_y - R_x L_y) S_x\big) x_{t_0-M} + (L_{xy} R_x - L_x R_{xy}) S_x \\ &+ (L_x R_{xx} - L_{xx} R_x) S_y + (L_{xx} R_{xy} - L_{xy} R_{xx})(N+M)\big| / d_C \\ a = &\big|(N M S_{xy} - M L_x L_y - N R_x R_y) x_{t_0-M}^2 \\ &+ \big|\big((L_x S_y + S_x L_y - (L_{xy} + S_{xy}) N) R_x + N R_{xx} R_y \\ &- M (R_{xx} L_y + L_x R_{xy})\big) x_{t_0-M} \\ &+ (L_{xy}(N+M) - L_x S_y) R_{xx} + R_x (-L_{xy} R_x + L_x R_{xy})\big| / d_C \\ b = &\big|((L_y S_{xx} - L_x S_{xy}) M + (L_x R_y - R_x L_y) R_x) x_{t_0-M}^2 \\ &+ \big|\big((L_x + S_x) L_{xy} - (S_y + L_y) L_{xx} + L_x R_{xy}) R_x \\ &- L_x R_y R_{xx} + L_{xx} R_{xy} M - L_{xy} R_{xx} M\big) x_{t_0-M} \\ &+ L_{xx}(S_y R_{xx} - R_{xy} R_x) - L_{xy} L_x R_{xx}\big| / d_C \\ d_C = &(N M S_{xx} - N R_x^2 - M L_x^2) x_{t0-M}^2 \\ &+ 2(L_x R_x S_x - M L_x R_{xx} - N R_x L_{xx}) x_{t0-M} \\ &- L_x^2 R_{xx} - R_x^2 L_{xx} + (N+M) L_{xx} R_{xx}\end{aligned} \tag{9}$$

Under the hypothesis H_0, Δ_a is an unbiased estimator for the corner size $E(\Delta_a) = 0 = a_r - a_l$ with variance

$$V(\Delta_a) = \frac{(N+M) S_{xx} - S_x^2}{d_C} \sigma_n^2 \quad . \tag{10}$$

In order to confirm a corner at some point in time $t_0 - M$, we need evidence for either the alternative that there is a positive corner H_{C+}: $\Delta_a > 0$ or the alternative that there is a negative corner H_{C-}: $\Delta_a < 0$ or the two-tailed alternative that there is some kind of a corner H_C: $\Delta_b \neq 0$. The corresponding hypothesis tests can easily be adapted from the jump detection (7) using the test statistic

$$t_C := \frac{\Delta_a}{\sqrt{V(\Delta_a)}} \tag{11}$$

C. Choosing the Parameters N and M

As the measured signal (x_t, y_t) cannot reveal itself based on any numbers of samples N and M without a sufficiently large change in the robots position x_t, N and M should be implicitly defined by fixing the constant lengths

$$L_L = x_{t_0-M} - x_{t_0-M-N+1} \quad \text{and} \quad L_R = x_{t_0} - x_{t_0-M+1}$$

Using these together with the robot speed v and the data sampling rate R, N and M are given respectively by

$$N = \frac{L_L}{v} R \quad \text{and} \quad M = \frac{L_R}{v} R$$

As the lengths L_L and L_R depend mostly on the given application and R is given by the sensor system, we need to adjust the robot speed v in order to achieve N and M large enough for the central limit theorems involved in the threshold calculations to hold. Note that the algorithm will not give reliable results before the end of its initialization length $L_L + L_R$ (or $N + M$) and that L_R (or M) determines the detection delay.

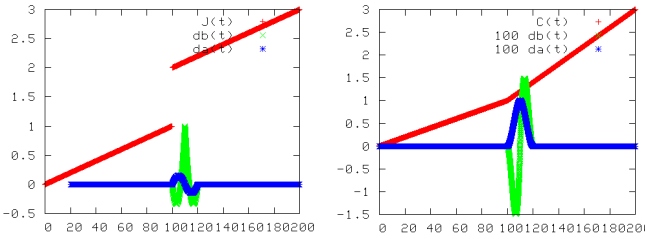

Fig. 5: Reactions $\Delta_b(t)$ (green) of the jump detector and $\Delta_a(t)$ (blue) of the corner detector to an ideal jump $J(t)$ (left) and to an ideal corner $C(t)$ (right)

D. Jump-Corner Distinction

Running the jump and the corner detection in parallel, it is easy to find the discontinuities in piecewise linear signals conforming to (1). Unfortunately, the jump and the corner detector react each to both jumps and corners with Δ_b and Δ_a differing from 0 respectively, making it difficult to classify a detected discontinuity (Fig. 5).

In order to get a correct classification and measurement of a detected discontinuity at some time t_d, the following $N + M$ detector outputs have to be taken into account. In fact, if the discontinuity is located exactly in the "middle" of the calculation interval ($x_{td-M} = x^*$), the expected values of the detectors correspond to the real sizes of the respective discontinuities, i.e. $E(\Delta_a) = a_r - a_l$ for $b_r = b_l - \Delta_a x^*$ and $E(\Delta_b) = b_r - b_l$ for $a_r = a_l$. Thus, only the output of the detectors around time $t_l + M$ in the interval starting with the first detection at t_l and ending with the last detection before time $t_l + N + M$ gives an approximation for the real size of the discontinuity in the signal. Note that this kind of classification can only be done $N + M$ samples after a discontinuity occurred.

IV. Experiments

A. Experiments on simulated data

The described algorithm is tested using data generated by the following function $S(x)$ with a corner of size –0.1 at $x = 100$ and a jump of size –1 at $x = 200$.

$$S(x) = \begin{cases} 0.2\,x & 0 \leqslant x < 100 \\ 0.1\,x + 10 & 100 \leqslant x < 200 \\ 0.1\,x + 9 & 200 \leqslant x < 300 \end{cases} \tag{12}$$

The data is sampled at a rate of 40 samples per unit of x. To each sample, a random number is added. The distribution for the random numbers is normal with mean 0 and standard deviation 0.5. The window lengths N and M are fixed to 400 samples each, thus covering 10 units of x. The signal, it's moving average over 200 samples (i. e. 5 units of x), and the calculated values for the test statistics t_J and t_C are depicted in Fig. 6. Additionally, a threshold of 4.0 corresponding to a confidence level of $\alpha = 0.007\%$ and the resulting detected corners and jumps are plotted over the data. With this confidence level, we can expect that less than 1 value of the 12000 ($12000\ \alpha = 0.84 < 1$) in the complete experiment fall outside the threshold, and, thus, that there will be no false detection.

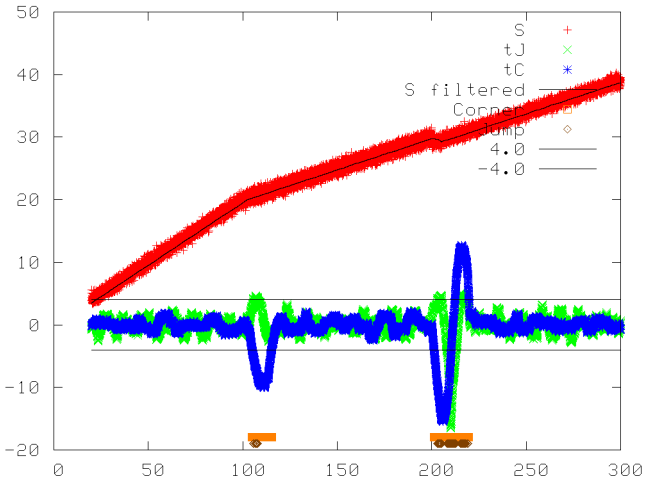

Fig. 6: Simulated data with a corner at $x = 100$ and a jump at $x = 200$ and calculated test statistics t_J and t_C with thresholds for $\alpha = 0.007\%$ and the resulting detected corners and jumps

B. *Experiments on real data*

The described algorithm is also tested on the example application from Section I (Fig. 2). The robot is a Stäubli RX 130 with a CS-7b controller from Adept. It is driven at a linear speed of $v = 10$ mm/s. As a sensor, a wrist-mounted 6D force/torque sensor 90M31A from JR3 is used. The data is sampled at the maximum possible rate of around $R = 400$ Hz. As the algorithm cannot distinguish between jumps and corners corresponding to friction and other unwanted effects, the operator needs to select the force signal with the best correspondence between detectable discontinuities and the wanted transitions between differently constrained situations.

For the localization of the endpoint on the plate, N and M are fixed by $L_L = L_R = 10$ mm. The raw data of the *Fy* force and *Mz* moment, each together with its moving average over an interval of length 5 mm (*Fy filtered* and *Mz filtered*), and the calculated values for the test statistics t_J and t_C are depicted in Fig. 7 and Fig. 8 respectively. In addition, the thresholds for the two-tailed alternatives H_J and H_C and the resulting detected jumps and corners are plotted over the data.

In the *Fy* force (Fig. 7), both the negative corner at 90 mm and the positive jump at 180 mm are safely recognized using a threshold of 1.0. In fact, the jump is recognized as two corners and three jumps, but in the middle of the corresponding interval of detected discontinuities, it can be classified as a positive jump.

In the *Mz* moment (Fig. 8), both of the real transitions are recognized correctly as corners using a threshold of 1.64. The first one is recognized as two jumps and a corner, but it can be classified correctly as a positive corner by the middle of the interval of detected discontinuities. Using lower thresholds, the curvature of the moment after the first corner is recognized as corners at 100 mm and at 125 mm. On the other side, higher thresholds may miss the second corner. Thus it is near impossible to choose a safe threshold for the Mz moment signal that detects the second corner without false alarms. Fortunately, monitoring the *Fy* force and the *Mz* moment signals at the same time with a high threshold of around 3, both transistions can be detected safely.

For the insertion of the endpoint into the slot, only the *Mz* moment can be used, as the *Fx* force is too much disturbed (Fig. 3). The point of insertion coincides clearly with the jump in the signal, so we can ignore all corners. That is why we choose a shorter N and M by $L_L = L_R = 5$ mm in order to better follow the small corners without erroneously interpreting them as jumps. The raw *Mz* moment, its moving average over 5 mm, the calculated test statistics t_J and t_C , the thresholds and the resulting detected corners and jumps are plotted in Fig. 9. The jump at 113 mm is correctly located by the detection algorithm as the test statistic t_J falls below the threshold –3. The jumps and corners detected directly before and after the real jump can be classified as side-effects.

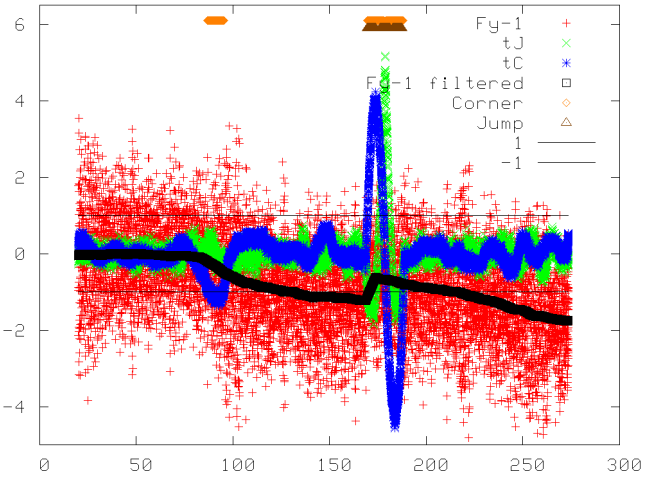

Fig. 7: *Fy* force signal and calculated decision signals for the endpoint localisation phase ploted against the robot location relative to its starting point: unfiltered data (red), moving average filtered data (black), test statistic for jump size (green), test statistic for corner size (blue), thresholds for $\alpha = 30\%$ and the intervals of detected jumps (brown) and corners (orange).

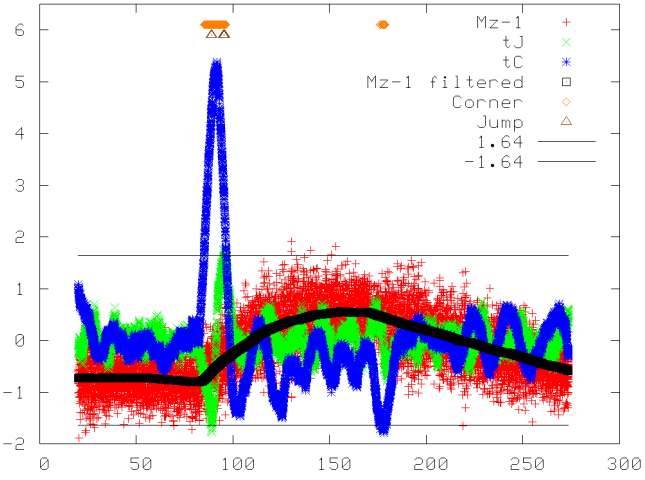

Fig. 8: *Mz* force signal and calculated decision signals for the endpoint localisation phase ploted against the robot location relative to its starting point: unfiltered data (red), moving average filtered data (black), test statistic for jump size (green), test statistic for corner size (blue), the thresholds for $\alpha = 10\%$ and the intervals of detected jumps (brown) and corners (orange).

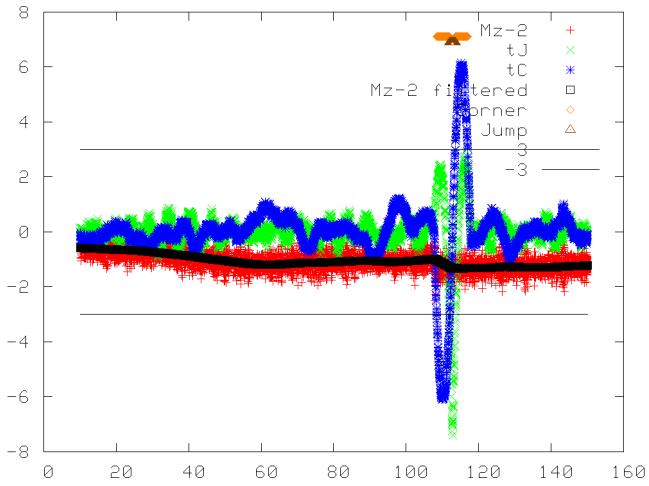

Fig. 9: *Mz* force signal and calculated decision signals for the endpoint insertion phase ploted against the robot location relative to its starting point: unfiltered data (red), moving average filtered data (black), test statistic for jump size (green), test statistic for corner size (blue), the thresholds for $\alpha = 0.3\%$ and the intervals of detected jumps (brown) and corners (orange).

Note that the presented thresholds of 1.0, 1.64 and 3.0 correspond to confidence levels of $\alpha = 30\%$, $\alpha = 10\%$ and $\alpha = 0.3\%$ respectively. But, as there are no false alarms at all using those low thresholds, we can assume that the measurement noise is not really white noise, and that the real confidence of those thresholds is much better.

V. Conclusions

As shown in the experiments section, both corners and jumps can be detected using our discontinuity detection algorithm. It has been seen, that curved signals may lead to false corner detections. If the curvature mostly remains buried in the noise and if the corner to be detected is much bigger than the curvature, false detections can be eliminated using another significance level α.

The proposed algorithm has low delay in detecting any discontinuity because the probability for detection starts to increase at the very moment, when a discontinuity enters the interval of calculations. Unfortunately, jumps may be seen as corners and corners as jumps when they enter respectively leave the interval of calculation. An exact decision can be found by checking the $N + M$ detector output values following a detection.

Compared to [7] our algorithm implements a completely continuous analysis of all the samples. In comparison to [4], it only uses constant computation time for each new signal sample, allowing to run it independently of N and M even on robot controllers with little computing power, provided that they can handle the constant calculation complexity involved in processing a signal sample at the minimum required sensor sampling rate.

Application of the algorithm is easy, as there are only three parameters controlling its operation. The first two are the numbers of samples N and M that should be fixed via L_L and L_R. It has been found, that $L_L = L_R$ varying between 5 and 10 mm (200 to 400 samples) is usually a good choice. Unless the robot speed is decreased or the sampling rate is increased, smaller values for L_L and L_R tend to produce noisier output but they allow the detectors to follow the signal more closely. The last parameter is the threshold for the test statistics. It should be set according to some desired significance level α for the case of raw data with normally distributed noise. For filtered data, an application specific threshold has to be chosen based on the real noise distribution. In both cases, optimal thresholds can be learned offline using some recorded force and moment data for different runs, each together with an operator's signaling about where the relevant discontinuities are located.

Of course, the algorithm cannot decide, whether a detected discontinuity corresponds to a desired transition between differently constrained situations or if it is due to friction or to some other unwanted effect. Thus, the most difficult remaining task for the robot programmer is to choose the most significant signal, i.e. the signal that is least disturbed while containing the minimum number of discontinuities needed in order to detect the desired transitions. This can be done according to [9].

Acknowledgements

This work has been supported by the German Research Foundation (DFG) under the project name: "Robot-based manipulation of deformable linear objects" (RODEO)

References

[1] Abegg F., Remde A., and Henrich D.: "Force- and vision-based detection of contact state transitions". In: Robot manipulation of deformable objects, Henrich D., Wörn H. (Eds.), Springer-Verlag, London, 2000, ISBN: 1-85233-250-6, pp. 111-134

[2] Desai, R. S. and Volz, R. A.: „Identification and Verification of Termination Conditions in Fine Motion in Presence of Sensor Errors and Geometric Uncertainties". In: 1989 IEEE Int. Conf. on Robotics and Automation (ICRA'89)

[3] Dutre, S., Bruyninckx, H. and De Schutter, J.: „Contact Identification and Monitoring Based on Energy". In: 1996 IEEE Int. Conf. on Robotics and Automation (ICRA'96)

[4] Lee, David: „Detection, Classification, and Measurement of Discontinuities". In: SIAM J. Sci. Stat. Comput. Vol. 12, No. 2, pp. 311-341, March 1991

[5] Morris G. H., Haynes L. S.: "Robotic assembly by constraints". In: Proc. 1987 IEEE Int. Conf. on Robotics and Automation (ICRA'87)

[6] Mosemann, H., Raue A., and Wahl, F.: „Classification and Recognition of Contact States for Force Guided Assembly". In: 1998 IEEE Int. Conf. on Systems, Man and Cybernetics

[7] Remde A., Pfaffenberger E., and Wörn H.: "Manipulating Deformable Linear Objects: Force-based Detection of Contact State Transitions". In: 2000 IEEE/RSJ Int. Conf. on Intelligent Robots and Systems (IROS'2000)

[8] Remde, A.: "Ein Ansatz zur Montage deformierbarer linearer Werkstücke mit Industrierobotern ". Dissertation. ISBN 3-89863-033-1, 2001, GCA-Verlag, Herdecke, Germany

[9] Schlechter, A., Henrich, D.: "Manipulating Deformable Linear Objects: Characteristics in Force Signals for Detecting Contact State Transitions". In: 2001 IEEE Int. Conf. On Advanced Robotics (ICAR'01)

[10] Wackerly, D. D., Mendenhall, W., Scheaffer, R.: "Mathematical Statistics with Applications", 6th Edition, Duxbury, USA, ISBN 0-534-37741-6

[11] Xiao, Jing: „Automatic Determination of Topological Contacts in the Presence of Sensing Uncertainties". In 1993 IEEE Int. Conf. on Robotics and Automation (ICRA'93)